Alternative RNA degradation pathways by the exonuclease Pop2p from *Saccharomyces cerevisiae*

XUAN YE,[1,2] ARMEND AXHEMI,[1,2] and ECKHARD JANKOWSKY[1,2,3]

[1]Center for RNA Science and Therapeutics, School of Medicine, Case Western Reserve University, Cleveland, Ohio 44106, USA
[2]Department of Biochemistry, School of Medicine, Case Western Reserve University, Cleveland, Ohio 44106, USA
[3]Case Comprehensive Cancer Center, School of Medicine, Case Western Reserve University, Cleveland, Ohio 44106, USA

ABSTRACT

The 3′ to 5′ exonuclease Pop2p (Caf1p) is part of the CCR4-NOT deadenylation complex that removes poly(A) tails from mRNAs in cells. Pop2p is structurally conserved in eukaryotes, but *Saccharomyces cerevisiae* Pop2p harbors noncanonical amino acids in its catalytic center. The enzymatic properties of *S. cerevisiae* Pop2p are not well defined. Here we characterize the RNA exonuclease activity of recombinant *S. cerevisiae* Pop2p. We find that *S. cerevisiae* Pop2p degrades RNAs via two alternative reactions pathways, one generating nucleotides with 5′-phosphates and RNA intermediates with 3′-hydroxyls, and the other generating nucleotides with 3′-phosphates and RNA intermediates with 3′-phosphates. The enzyme is not able to initiate the reaction on RNAs with a 3′-phosphate, which leads to accumulation of RNAs with 3′-phosphates that can exceed 10 nt and are resistant to further degradation by *S. cerevisiae* Pop2p. We further demonstrate that *S. cerevisiae* Pop2p degrades RNAs in three reaction phases: an initial distributive phase, a second processive phase and a third phase during which processivity gradually declines. We also show that mutations of subsets of amino acids in the catalytic center, including those previously thought to inactivate the enzyme, moderately reduce, but not eliminate activity. Only mutation of all five amino acids in the catalytic center diminishes activity of Pop2p to background levels. Collectively, our results reveal robust exonuclease activity of *S. cerevisiae* Pop2p with unusual enzymatic properties, characterized by alternative degradation pathways, multiple reaction phases and functional redundancy of amino acids in the catalytic core.

Keywords: RNA; nuclease; processivity; deadenylation

INTRODUCTION

Saccharomyces cerevisiae Pop2p (Caf1p) is a 3′ to 5′ exonuclease (Thore et al. 2003). The enzyme is part of the CCR4-NOT deadenylation complex that removes poly(A) tails from mRNAs in cells (Daugeron et al. 2001; Parker 2012; Collart and Panasenko 2017; Tang and Passmore 2019). Like other components of the CCR4-NOT deadenylation complex, Pop2p is conserved in eukaryotes (Basquin et al. 2012; Winkler and Balacco 2013; Collart and Panasenko 2017). Pop2p belongs to the DEDD family, which derive their name from a set of characteristic, widely conserved amino acids in the catalytic center of the enzymes (Zuo and Deutscher 2001; Bianchin et al. 2005; Ibrahim et al. 2009). However, in *S. cerevisiae* Pop2p, three out of five of these characteristic amino acids are not present (S188, Q394, and T389), even though structural data indicate correct assignment of *S. cerevisiae* Pop2p to the DEDD family (Thore et al. 2003; Jonstrup et al. 2007; Andersen et al. 2009; Horiuchi et al. 2009; Basquin et al. 2012).

Despite its noncanonical catalytic center, the exonuclease domain of *S. cerevisiae* Pop2p degrades poly(A) and other RNAs 3′ to 5′ in vitro, as expected for a DEDD exonuclease (Daugeron et al. 2001; Thore et al. 2003) and similar to Pop2p orthologs (Viswanathan et al. 2004; Jonstrup et al. 2007; Schwede et al. 2008; Andersen et al. 2009; Horiuchi et al. 2009; Temme et al. 2010; Niinuma et al. 2016). Mutations of critical amino acids in the catalytic center of Pop2p orthologs inactivate the enzymes and reduce cellular deadenylation, indicating that Pop2p activity is critical in the corresponding organisms (Niinuma et al. 2016; Balagopal et al. 2017; Webster et al. 2018; Yi et al. 2018). In *S. cerevisiae* Pop2p, however, the link between exonuclease activity

Corresponding author: exj13@case.edu
Article is online at http://www.rnajournal.org/cgi/doi/10.1261/rna.078006.120.

and cellular function is not clear. Mutation of two amino acids that are presumed to be essential for Pop2p activity (S188 and E190), based on structural studies and similarities to canonical DEDD exonucleases, reduced activity in vitro (Jonstrup et al. 2007; Andersen et al. 2009; Horiuchi et al. 2009; Niinuma et al. 2016; Webster et al. 2018; Yi et al. 2018; Raisch et al. 2019; Tang et al. 2019). Yet, introduction of these mutations in *S. cerevisiae* cells had little impact on deadenylation in cells (Viswanathan et al. 2004; Balagopal et al. 2017). Deletion of *pop2* and interruption of the Pop2p–Not1p interaction, however, result in slow growth, which is exacerbated at elevated temperatures (Tucker et al. 2001, 2002; Basquin et al. 2012; Webster et al. 2018). For these reasons, Pop2p has been thought to play a predominantly structural role in the CCR4-NOT complex during mRNA deadenylation in *S. cerevisiae* (Tucker et al. 2001, 2002; Basquin et al. 2012; Winkler and Balacco 2013). In other organisms, Pop2p is considered a major, if not the predominant exonuclease of the CCR4-NOT complex (Temme et al. 2004, 2010; Schwede et al. 2008).

Although Pop2p's RNase domain has been qualitatively shown to degrade RNA with 3′ to 5′ polarity, the exonuclease activity of *S. cerevisiae* Pop2p has not been characterized in depth. This absence of biochemical data, combined with the intriguing difference in the presumed cellular function of the enzyme in *S. cerevisiae*, compared with other organisms, motivated us to characterize the exonuclease activity of full-length *S. cerevisiae* Pop2p in vitro.

We show that *S. cerevisiae* Pop2p produces terminal RNA products that are markedly longer than those seen with other exonucleases. The length of these terminal products depends on the length of the initial substrate and can exceed 10 nt for substrates with more than 20 nt. We further find that *S. cerevisiae* Pop2p produces both, 5′-phosphorylated and 3′-phosphorylated nucleotides during the reaction and RNA intermediates that contain either 3′-hydroxyls (3′-OH) or 3′-phosphates. However, the enzyme is not able to initiate the reaction on RNAs with a 3′-phosphate. We discover that the degradation reaction for RNAs with 24 or more nucleotides occurs in three phases: an initial distributive phase, a second processive phase and a third phase during which processivity gradually declines. We also show that *S. cerevisiae* Pop2p degrades non-poly(A) substrates efficiently, but displays a preference for substrates with stretches of poly(A). Finally, we demonstrate that mutation of amino acids in the catalytic center that were previously thought to inactivate the enzyme, diminish, but do not eliminate activity. Mutations of other subsets of amino acids in the catalytic center also result in moderate reductions of activity. Only mutation of all five amino acids in the catalytic center reduces activity of Pop2p to background levels. Collectively, the data reveal robust exonuclease activity of *S. cerevisiae* Pop2p, but unusual enzymatic properties, characterized by alternative degradation pathways that produce 3′- and 5′-phosphorylated nucleotides, and by functional redundancy of amino acids in the catalytic core.

RESULTS

Pop2p generates long terminal products.

To characterize the exonuclease activity of Pop2p, we measured RNA degradation in vitro with excess enzyme over an RNA substrate with 36 adenylates (A_{36}, Fig. 1A; for all substrate sequences please see Table 1, Materials and Methods). We observed shortening of the substrate over time and pronounced accumulation of RNAs with 10–16 nt (Fig. 1B). RNAs of similar length also accumulated in reactions at a higher ratio of Pop2p to RNA (Fig. 1C) and at different reaction conditions (Supplemental Figs. S1, S2). We next measured degradation of a substrate with 24 adenylates (A_{24}, Fig. 1D). We detected accumulation RNAs with 8–16 nt (Fig. 1D), including slightly shorter species than seen with A_{36} (Fig. 1B). This observation suggested an influence of the initial substrate length on the length of the accumulating RNAs.

To further test this notion, we probed degradation of an RNA with 13 adenylates (A_{13}). We observed accumulation of RNAs with 6–11 nt (Fig. 1E), markedly shorter species than seen with A_{36} and A_{24} (Fig. 1F). Apparent reaction rate constants at identical enzyme concentrations were higher for A_{36}, and A_{24}, compared with A_{13} (Fig. 1G). Yet, Pop2p readily processed all three substrates. The reaction of A_{13} is notable because RNAs with 13 nt fall into the range of RNAs that accumulate in reactions of A_{36} and A_{24} (Fig. 1B–D). Collectively, these data indicate that RNA degradation by Pop2p produced terminal products with lengths that scale with the initial substrate length. However, for all tested substrates the lengths of these terminal products markedly exceed the minimal RNA binding site of Pop2p extrapolated from crystal structures, which covers ~5 nt.

Pop2p generates nucleotides with 3′ and 5′ phosphates

Accumulation of RNAs with lengths that depend on the length of the starting substrates had not been reported for RNA exonucleases, to our knowledge. We therefore investigated the molecular basis for this phenomenon. We first tested whether inactivation of Pop2p during the reaction or nonproductive binding of Pop2p to the terminal products accounted for our observations. Nonproductive RNA binding, which has been demonstrated for the DEDD RNA exonuclease Rrp6p, causes accumulation of RNAs with 16–19 nt during the degradation reaction (Axhemi et al. 2020). However, Rrp6p eventually degrades these accumulated RNAs and the lengths of the accumulating RNAs do not scale with the initial substrate length (Axhemi et al. 2020).

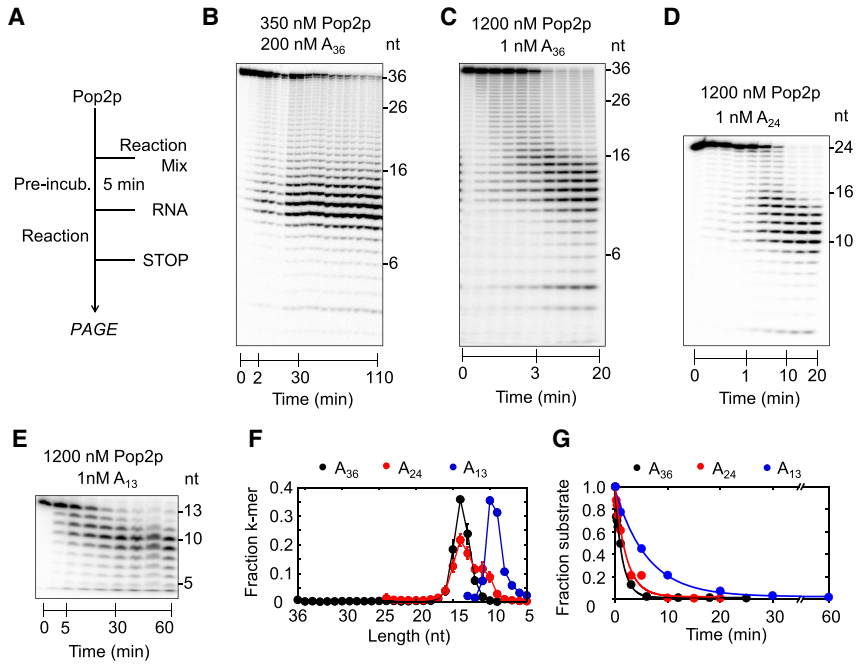

FIGURE 1. Degradation of poly(A) RNA by *S. cerevisiae* Pop2p. (*A*) Reaction scheme for pre-steady-state exonuclease reaction by Pop2p. (*B*) Representative PAGE for a pre-steady-state exonuclease reaction with A_{36}. Aliquots were removed at 0.5, 2, 5, 10, 15, 20, 25, 30, 35, 40, 45, 50, 60, 70, 80, 90, 100, and 110 min. Numbers indicate the RNA length. (*C*) Representative PAGE for a pre-steady-state exonuclease reaction with A_{36} with increased ratio of Pop2p to RNA. Aliquots were removed at 10, 20, 40 sec, 1, 3, 5, 10, 15, and 20 min. (*D*) Representative PAGE for a pre-steady exonuclease reaction with A_{24}. Aliquots were removed at 10, 20, 40 sec, 1, 3, 5, 10, 15, and 20 min. (*E*) Representative PAGE for a pre-steady exonuclease reaction with A_{13}. Aliquots were removed at 1, 5, 10, 20, 30, 40, 50, and 60 min. (*F*) Distribution of *k*-mers (length of remaining substrate species) at the 20 min time point for pre-steady exonuclease reactions (Pop2p: 1200 nM) with indicated RNA substrates. Data points represent an average of three independent experiments. Error bars show one standard deviation. (*G*) Time courses for removal of the 3′ nucleotide of the initial substrate degradation for the reactions shown in panels *C*–*E*. The curves were fitted to integrated rate for an irreversible first order reaction ($k_{obs}^{(A36)} = 0.71 \pm 0.10\ min^{-1}$, $k_{obs}^{(A24)} = 0.47 \pm 0.06\ min^{-1}$, $k_{obs}^{(A13)} = 0.16 \pm 0.01\ min^{-1}$).

To probe for nonproductive binding of Pop2p to the accumulating RNAs and for the possibility that Pop2p became inactivated during the course of the reaction, we performed the reaction, followed by heat inactivation of Pop2p and addition of new Pop2p to the reaction (Fig. 2A,B). We observed no further degradation of the accumulated RNAs by newly added Pop2p (Fig. 2B). These observations are inconsistent with nonproductive binding of Pop2p to the accumulating RNAs during the reaction and rule out Pop2p inactivation during the course of the reaction.

We next isolated the accumulated RNA species and added new Pop2p (Fig. 2C,D). Again, we observed no degradation of the accumulated RNAs (Fig. 2D). In contrast, the *S. cerevisiae* exonuclease Rrp44p readily degraded the accumulated RNAs (Fig. 2D), indicating that the substrate isolation procedure did not interfere with exonuclease reactions per se. These results further support the notion that accumulation of RNA with more than 10 nt was not due to nonproductive Pop2p binding to these RNAs and not due to inactivation of Pop2p during the reaction.

The data indicated that Pop2p was unable to degrade RNAs that had been produced during the reaction. In contrast, an unreacted substrate with 13 adenylates (A_{13}) was readily degraded (Fig. 1E). The difference between reacted and unreacted RNAs led us to hypothesize that the RNAs accumulating during the reaction of Pop2p differed chemically from unreacted RNAs. To test this hypothesis, we generated a substrate with internal ^{32}P radiolabels (Fig. 2E,F), subjected this RNA to a reaction with Pop2p and analyzed the degradation products by thin layer chromatography (TLC) and PAGE (Fig. 2F,G). In parallel, we analyzed a degradation reaction with Rrp44p (Fig. 2F,G). For both, Pop2p and Rrp44p, accumulation of monophosphates is seen on TLC (Fig. 2G), which correlated with the observed substrate degradation seen on PAGE (Fig. 2H). This correlation shows that all reaction products containing a phosphate are visible on TLC.

For Rrp44p, we observed almost exclusive accumulation of a single nucleotide species on TLC (Fig. 2G). Since Rrp44p produces predominantly 5′-AMP during the reaction (Zinder et al. 2016), we concluded that this species represents 5′-AMP. Treatment with Antarctic Phosphatase converted the 5′-AMP into phosphate (Fig. 2G), as expected (Rina et al. 2000). For Pop2p, we observed accumulation of 5′-AMP and an additional species (Fig. 2G). Both, the 5′-AMP and the additional species were converted to phosphate by Antarctic Phosphatase (Fig. 2G), indicating that both species contained a terminal, noncyclic phosphate (Das and Shuman 2013). Since this terminal phosphate could only be attached to 5′ (5′-AMP) or 3′ (3′-AMP), we concluded that the additional species in the Pop2p reaction represents a 3′-AMP. The data thus revealed that Pop2p generated two distinct phosphorylated nucleotide products, a 5′-AMP and a 3′-AMP.

Pop2p uses two alternative degradation pathways

The generation of two phosphorylated nucleotide degradation products suggested a scenario where Pop2p degrades RNA via two alternative pathways (Fig. 3).

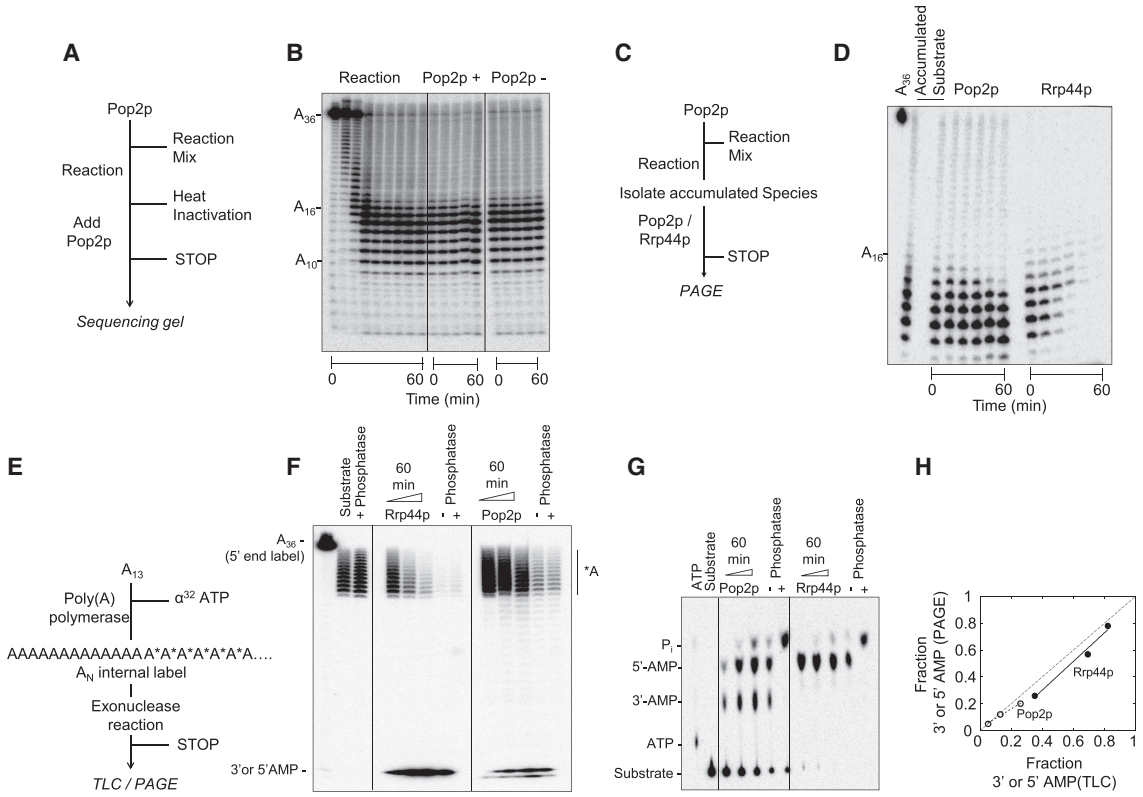

FIGURE 2. Distinct reaction products during RNA degradation by Pop2p. (*A*) Reaction scheme for Pop2p exonuclease reaction with addition of new Pop2p. (*B*) Representative PAGE for an exonuclease reaction with A_{36} and addition of new Pop2p. Pre-steady-state exonuclease reaction (Pop2p: 1200 nM, A_{36}: 1 nM, aliquots were removed at 1, 5, 10, 20, 30, 40, 50, and 60 min), followed by heat inactivation of Pop2p at 60 min (65°C, 20 min) and addition of fresh Pop2p (1200 nM). Aliquots were removed after addition of fresh Pop2p at 15, 30, 40, 50, and 60 min (*middle*). (*Right*) Control reaction without addition of fresh Pop2p after heat inactivation. (*C*) Reaction scheme for Pop2p exonuclease reaction with terminal reaction products. (*D*) Representative PAGE for an exonuclease reaction of Pop2p (1200 nM) and Rrp44p (1200 nM) with isolated, terminal reaction products (1 nM). Aliquots were removed at 15, 30, 40, 50, and 60 min. (*E*) Reaction scheme for generation of the internally radiolabeled RNA and for the Pop2p exonuclease reactions with this substrate. The asterisks represent the radiolabeled ^{32}P linkages between adenosines. (*F*) Representative PAGE for exonuclease reactions of Rrp44p (1200 nM) and Pop2p (1200 nM) with internally radiolabeled RNA substrate (aliquots: 15, 30, and 60 min). Products generated after 60 min were treated with Antarctic Phosphatase. (*G*) Representative TLC for Pop2p and Rrp44p exonuclease reactions with internally radiolabeled RNA substrate (aliquots: 15, 30, and 60 min). Products generated after 60 min were treated with Antarctic Phosphatase. (*H*) Correlation of the fraction monophosphate (5′-AMP + 3′-AMP vs. unreacted product) generated during the reaction (time points: 15, 30, and 60 min) measured by TLC and PAGE.

However, two alternative degradation pathways could not explain the inability of Pop2p to degrade RNAs produced in the reaction, while degrading unreacted RNA substrates of identical length. The 3′-AMP produced during the reaction indicated that Pop2p could degrade RNA with 3′-phosphates (Fig. 2G). However, formation of 3′-AMP and inability to process reacted substrates could be reconciled if Pop2p was unable to initiate a reaction on RNA with 3′-phosphates, but degraded these RNAs after initiating the reaction on an RNA with a 3′-OH. A degradation reaction with these features would have to rely on two characteristics: first, an inability of Pop2p to initiate a reaction on RNAs with 3′-phosphates, and second, a degree of processivity, that is, the ability of the enzyme to perform multiple degradation steps without dissociating from the RNA (Kelman et al. 1998; Jankowsky et al. 2000; Fairman-Williams and Jankowsky 2012).

We set out to test these two characteristics. We first examined the ability of Pop2p to initiate a degradation reaction on an A_{13} substrate with a 3′-phosphate (Fig. 4A,B). We did not observe significant degradation of the substrate with the 3′-phosphate, while identical RNAs with 3′-OH were readily degraded (Fig. 4C). Identical observations were made with an A_{24} substrate (Fig. 4C). These results show that Pop2p is not able to initiate the reaction on RNAs with a 3′-phosphate.

Pop2p degrades RNA processively in a multiphasic reaction

We next tested whether Pop2p degrades RNAs processively. To this end we performed pulse-chase experiments, where scavenger RNA was added after the reaction start (Fig. 5A). The scavenger prevents Pop2p that dissociates

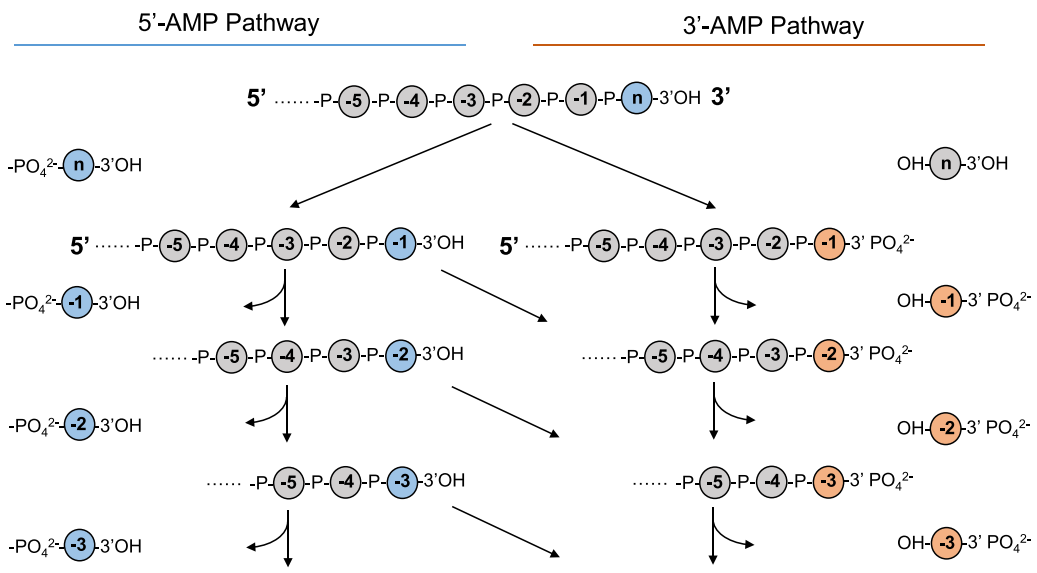

FIGURE 3. Alternative RNA degradation pathways by Pop2p. Model of the two simultaneous degradation pathways of the Pop2p. Spheres represent the nucleoside, P the phosphodiester linkage between nucleotides.

from the substrate after scavenger addition to rebind the substrate (Jia et al. 2011; Axhemi et al. 2020). Continuation of the reaction past scavenger addition indicates processivity (Jia et al. 2011; Axhemi et al. 2020). We observed continuation after scavenger addition (Fig. 5B; Supplemental Fig. S3), indicating processive degradation by Pop2p. Quantification of the pulse-chase reactions for A_{36} and A_{24} revealed a gradual increase in processivity, followed by a gradual decrease (Fig. 5C). On A_{36}, Pop2p is more likely to dissociate from the RNA than to continue for the first three steps ($P < 0.5$), although processivity increased from steps 1 to 3 (Fig. 5C). For the next nine steps, processivity increased to a value of $P = 0.88 \pm 0.09$, indicating up to approximately 8 degradation steps per binding event (Fig. 5C). Processivity then gradually decreased (Fig. 5C). On A_{24}, Pop2p processivity also increased from low values and then gradually decreased (Fig. 5C). The maximal processivity was lower than for A_{36} and fewer steps were taken with high processivity. Nevertheless, processivity on reaction intermediates with less than 21 adenylates was higher for A_{24} than for A_{36} (Fig. 5C).

Collectively, these observations indicate that Pop2p can processively degrade RNAs. The complex dependence of the processivity on the RNA length reveal multiple phases of the Pop2p reaction. Pop2p traverses an initial distributive phase before entering a processive mode, similar to other enzymes that act processively on nucleic acids (Kelman et al. 1998; Jankowsky et al. 2000; Fairman-Williams and Jankowsky 2012). However, Pop2p maintains processivity only for several steps. The number of highly processive steps ($P > 0.5$) appears to decrease for a substrate with shorter starting length, suggesting that Pop2p can sense either the length of the remaining RNA, the substrate starting length, or both.

The gradual decrease in processivity after several steps coincides with the emergence of reaction intermediates with 3′-phosphates that are resistant to further Pop2p

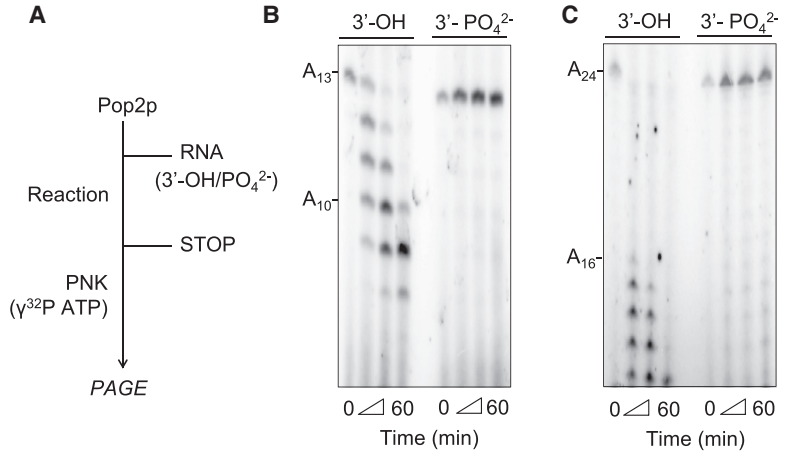

FIGURE 4. Inability of Pop2p to degrade RNA with 3′ phosphate. (*A*) Reaction scheme for the Pop2p exonuclease reaction on poly(A) substrates containing either 3′-PO_4 or 3′-OH. (*B*) Representative PAGE for an exonuclease reaction of Pop2p (1200 nM) with A_{13} (1 nM) with either 3′-PO_4 or 3′-OH. Aliquots were removed at 5, 15, and 60 min. (*C*) Representative PAGE for an exonuclease reaction of Pop2p (1200 nM) with A_{24} (1 nM) with either 3′-PO_4 or 3′-OH. Aliquots were removed at 5, 15, and 60 min.

degradation (Figs. 1, 2). This correlation is consistent with the notion that Pop2p can degrade RNAs with 3′-phosphates in the processive mode. The data further suggest that the alternative cleavage pathways (Fig. 3) are not evenly populated for each reaction step, otherwise the accumulation of the 3′-phosphate RNAs would roughly mirror the processivity plot and intermediates with 3′-phosphates would accumulate at the reaction start, which is not observed (Fig. 1). The data suggest that intermediates with 3′-phosphates are formed either during the processive phase, during the phase where processivity decreases, or during both phases, with potentially differing frequencies. A scenario with multiple reaction phases, but no formation of reaction intermediates with 3′-phosphates during the initial phase is supported by observations made with A_{13}, for which Pop2p removes only a few nucleotides (Fig. 1). The processivity of Pop2p and its inability to initiate the reaction on substrates with 3′-phosphates reconciles the ability of Pop2p to generate 3′ and 5′ AMP and the accumulation of terminal reaction products that scale in length with the initial substrate length.

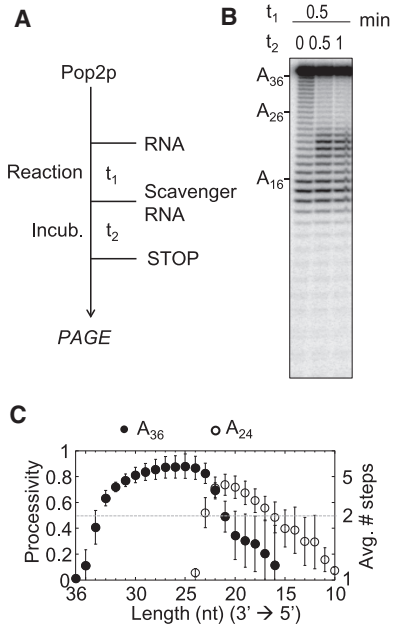

FIGURE 5. Processive RNA degradation by Pop2p. (*A*) Reaction scheme for pulse-chase experiments. (*B*) Representative PAGE for a pulse-chase reaction of Pop2p (1200 nM) with A_{36} (1 nM) and scavenger RNA (5 μM). (t_1: reaction time after addition of labeled substrate. t_2: incubation time after addition of scavenger RNA). (*C*) Processivity values of Pop2p for A_{36} and A_{24} RNA substrates. Data points represent the average of three independent experiments, error bars show one standard deviation. The average number of steps (*right* axis) was calculated according to $P = (N-1)N^{-1}$ (P: processivity value, N: average number of steps) (Axhemi et al. 2020).

RNA sequence impacts Pop2p activity

Having established that Pop2p utilizes an unusual exonuclease mechanism that combines alternative degradation pathways in a multiphasic reaction, we next examined the impact of RNA sequence on the activity of Pop2p. By virtue of its association with the CCR4-NOT complex, Pop2p is thought to primarily act on poly(A) RNA. However, recombinant Pop2p was qualitatively shown to also degrade other RNA sequences (Daugeron et al. 2001; Thore et al. 2003).

To obtain a more detailed picture of possible sequence preferences of Pop2p activity, we first characterized degradation of homopolymeric U_{36} and C_{36} substrates under the pre-steady-state conditions used to examine poly(A) substrates (Fig. 6A). A homopolymeric G substrate was not tested because of the propensity to form G-quadruplex structures (Sengar et al. 2014). Pop2p readily degraded U_{36} and C_{36} substrates (Fig. 6A), as well as a substrate with mixed A/U sequence (Supplemental Fig. S4). Terminal products similar to those seen with A_{36} were detected, although their distribution for U_{36} and C_{36} was shifted to slightly longer species, compared to A_{36} (Fig. 6A). At identical enzyme concentrations, Pop2p degraded the U_{36} and C_{36} substrates slower than A_{36} (Fig. 6B). These data suggest either weaker functional binding of Pop2p or slower degradation rate at enzyme saturation for U_{36} and C_{36}, compared to A_{36}. We were unable to further distinguish between these two possibilities, because saturating enzyme concentrations could not be experimentally realized. Nevertheless, our data indicate an inherent preference of Pop2p for adenylate RNA over other, homopolymeric RNAs.

We also measured the processivity of Pop2p on C_{36} and U_{36} (Fig. 6C). The data revealed multiple reactions phases, as seen for A_{36}. However, the first phase, wherein processivity increases over several reaction steps is markedly longer for U_{36} and C_{36}, compared to A_{36}. The second "processive" phase is shorter and maximal processivity is lower for U_{36} and C_{36} than for A_{36}. The third phase, where processivity gradually declines, is similar for all three substrates (Fig. 6C).

The data collectively indicate that Pop2p can degrade nonadenylate RNA with functional characteristics similar to poly(A) substrates. Higher degradation rates at identical enzyme concentrations and higher processivity for poly(A) substrates, compared with poly(C) and poly(U) substrates suggests an inherent preference of Pop2p for poly(A) over other homopolymeric RNA.

We next characterized Pop2p activity on 36 nt substrates consisting of fused C and A homopolymers (5′-$C_{26}A_{10}$-3′, 5′-$A_{26}C_{10}$-3′, Fig. 6D). Pop2p readily degraded both substrates (Fig. 6D). Characteristic long terminal products were again detected, although their length distribution differed (Fig. 6D). At identical enzyme concentrations, the substrate with 3′-terminal adenylates (5′-$C_{26}A_{10}$-3′) reacted faster than the substrate with 3′-terminal cytidines

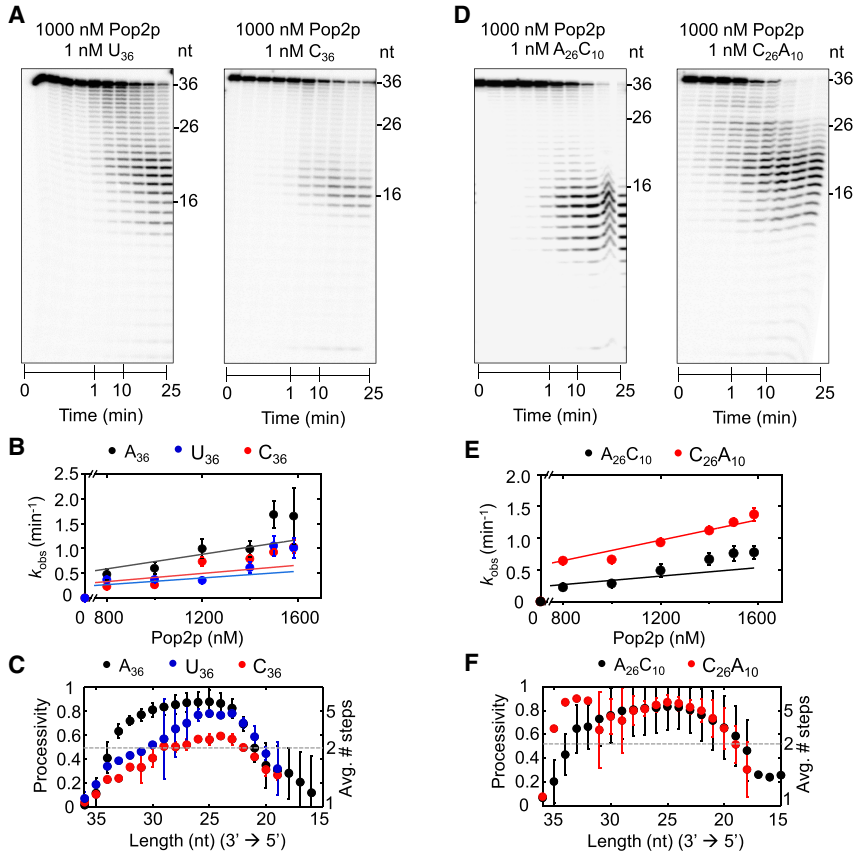

FIGURE 6. Sequence effects on exonuclease activity of Pop2p. (*A*) Representative PAGE for an exonuclease reaction of Pop2p (1000 nM) with U_{36} and C_{36} (1 nM). Aliquots were removed at 10, 20, 40 sec, 1, 5, 10, 15, 20, and 25 min. (*B*) Observed rate constants (removal of first nucleotide) for degradation of C_{36} and U_{36} as a function of Pop2p concentration. Data for A_{36} are given for comparison. Error bar represents the standard error from fitting time courses to rate equations. (*C*) Processivity values of Pop2p for U_{36} and C_{36} (data for A_{36} are given for comparison). Data points represent an average of three independent experiments, error bars show one standard deviation. Numbers indicate the average number of steps. (*D*) Representative PAGE for an exonuclease reaction of Pop2p (1000 nM) with $A_{26}C_{10}$ and $C_{26}A_{10}$. Aliquots were removed at 10, 20, 40 sec, 1, 5, 10, 15, 20, and 25 min. (*E*) Observed rate constants (removal of first nucleotide) for degradation of $A_{26}C_{10}$ and $C_{26}A_{10}$ as a function of Pop2p concentration. Error bar represents the standard error from fitting time courses to rate equations. (*F*) Processivity values of Pop2p for $A_{26}C_{10}$ and $C_{26}A_{10}$. Data points represent an average of three independent experiments, error bars show one standard deviation. Numbers indicate the average number of steps.

(5′-$A_{26}C_{10}$-3′, Fig. 6E). Processivity measurements on these substrates again revealed the three characteristic reaction phases that were seen for the other substrates (Fig. 6F). The plot of processivity values versus RNA length for the substrate with 3′-terminal cytidines (5′-$A_{26}C_{10}$-3′) was highly similar to the plot with the A_{36} substrate (Fig. 6F). Notably, the plot for the substrate with 3′-terminal adenylates (5′-$C_{26}A_{10}$-3′) showed a shorter first phase, a longer second phase and higher maximal processivity values, compared with the A_{36} and the 5′-$A_{26}C_{10}$-3′ substrates (Fig. 6F). These data highlight an unexpected interplay between 3′-terminal and upstream sequences for the degradation reaction. While 3′-terminal adenylates are critical for fast degradation, processivity is affected by both, 3-terminal and downstream sequence. Stretches of adenylates, either 3′-terminal or downstream, promote degradation. The length distribution of the terminal products also appears to be affected by the downstream sequence. Collectively, our data show that Pop2p readily degrades non-poly(A) RNAs. Functional characteristics of Pop2p on these substrates are similar to those seen for poly(A) substrates, but Pop2p prefers substrates with adenylate stretches.

Mutational analysis of the catalytic core

Our data above highlighted unusual features of the exonuclease activity of Pop2p. Given that the catalytic core of Pop2p is comprised of noncanonical catalytic residues, we examined how key residues in the catalytic core contributed to the function of the enzyme. We generated four Pop2p constructs with mutations in the five amino acids in the catalytic core (Fig. 7A).

$Pop2p^{(S188A,E190A)}$, which had been previously examined (Tucker et al. 2002; Thore et al. 2003; Viswanathan et al. 2004; Balagopal et al. 2017), retained significant activity, although at a reduced level, compared with wild-type (wt) Pop2p (Fig. 7B,C). We also observed long terminal products, as seen for wt Pop2p (Fig. 7B). These results suggested that substitution of S188 and E190 with alanines did not fundamentally alter the degradation mechanism. Retention of significant activity by $Pop2p^{(S188A,E190A)}$ is notable, because this Pop2p variant has been used in several studies as inactive control (Viswanathan et al. 2004; Balagopal et al. 2017). The clear exonuclease activity associated with $Pop2p^{(S188A,E190A)}$ might require reassessment of conclusions regarding Pop2p roles in these studies.

$Pop2p^{D310A}$ also retained exonuclease activity, but at a lower level than $Pop2p^{(S188A,E190A)}$ (Fig. 7C). Long RNAs accumulated, suggesting that the D310A mutation also did not fundamentally alter the degradation mechanism of Pop2p. However, the accumulating RNAs were longer than for wtPop2p and Pop2p $Pop2p^{(S188A,E190A)}$,

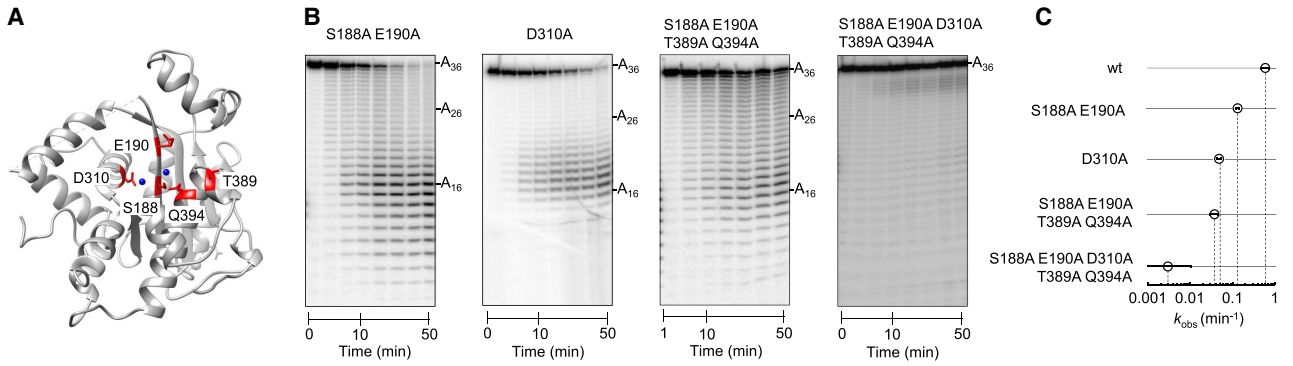

FIGURE 7. Exonuclease activity of mutant Pop2p variants. (*A*) Structure of the *S. cerevisiae* Pop2p exonuclease domain (PDB: 1UOC). Blue spheres represent the Mg^{2+} ions extrapolated from the *S.p.* Pop2p exonuclease domain (PDB: 2P51). Amino acids in the catalytic center are marked red. (*B*) Representative PAGE for exonuclease reactions of Pop2p variants (as indicated) (1000 nM) with A_{36} (1 nM). Aliquots were removed at 1, 5, 10, 20, 30, 40, and 50 min. (*C*). Observed rate constants (removal of first nucleotide) for degradation of A_{36} with the Pop2p variants indicated. Error bar represents the standard error from fitting time courses to rate equations.

highlighting potential changes in the balance between the pathways producing RNAs with 3′-phosphate and 3′-OH, compared with wt Pop2p.

We next replaced four amino acids, S188, E190, T389, and Q394 with alanines. The resulting $Pop2p^{(S188A,E190A,T389A,Q394A)}$ still showed measurable, yet diminished activity, compared to wt Pop2p and the two variants tested above. (Fig. 7B,C). Accumulation of long RNA products was still detectable. The data indicate that even a change of four of the five catalytic residues does not completely abolish the Pop2p activity. We finally replaced all five amino acids with alanine. The activity of the resulting $Pop2p^{(S188A,E190A,D310A,T389A,Q394A)}$ was reduced close to background level (Fig. 7B,C). Collectively, our data highlight a remarkable resilience of Pop2p against mutations of residues in the catalytic core. A drastic change of five amino acids is required to virtually eliminate activity.

DISCUSSION

Our characterization of Pop2p from *S. cerevisiae* reveals alternative degradation pathways that produce nucleotides with 3′ and 5′ phosphates, a reaction with multiple phases of differing processivity, and the inability of the enzyme to initiate the reaction on substrates containing a 3′-phosphate. Together, these features cause termination of the degradation reaction after a limited number of nucleotides and generate reaction products markedly longer than the minimal Pop2p binding site on RNA, extrapolated from crystal structures. Instead, the length of these reaction products depends on the length of the initial substrate and the RNA sequence.

We are not aware of reports describing similar characteristics for other RNA exonucleases. We therefore speculate that Pop2p from *S. cerevisiae* has unusual, as of yet unknown roles during RNA degradation, provided the in vitro characteristics of Pop2p are not fundamentally altered in the CCR4-NOT complex. In cells, the 3′-phosphate on RNAs might serve as chemical mark on RNAs that Pop2p has processed, perhaps constituting a fail-safe mechanism that prevents multiple rounds of degradation of a given RNA by Pop2p. Alternatively, the chemical mark might serve as checkpoint for other processing enzymes. Both scenarios are not mutually exclusive.

In addition to revealing unusual enzymatic features, our data show pronounced exonuclease activity of Pop2p, including processive RNA degradation. These data suggest that it is unlikely that Pop2p in *S. cerevisiae* functions solely as architectural component of the CCR4-NOT complex, although our findings do not rule out such a role. However, the marked activity of $Pop2p^{(S188A,E190A)}$, a variant that has been considered inactive, might require reevaluation of at least some conclusions from previous studies that assumed loss of function for $Pop2p^{(S188A,E190A)}$. Collectively, our findings emphasize that further work is required to delineate the cellular roles of Pop2p from *S. cerevisiae*.

Pronounced and processive exonuclease activity is seen for Pop2p orthologs from other organisms, where the enzyme is considered a main poly(A) degradation protein (Daugeron et al. 2001; Viswanathan et al. 2004; Bianchin et al. 2005; Horiuchi et al. 2009; Niinuma et al. 2016). The preference of *S. cerevisiae* Pop2p for poly(A) also mirrors poly(A) preferences of Pop2p orthologs (Bianchin et al. 2005; Horiuchi et al. 2009; Niinuma et al. 2016). However, *S. cerevisiae* Pop2p shows clear activity on non-poly(A) RNA, indicating that the enzyme is capable of processing RNAs other than polyadenylated mRNAs. It is possible that the 3′-phosphate serves to prevent Pop2p from extensively degrading mRNAs from which the poly(A) tail has already been removed. Notably, a sizable fraction of mRNAs without poly(A) tails appears to accumulate in *S. cerevisiae* (Daugeron et al. 2001; Tucker et al. 2001, 2002). It is not known whether or not these mRNAs contain 3′-phosphates.

The multiphasic reaction of *S. cerevisiae* Pop2p is similar to reaction characteristics seen for enzymes that act processively on nucleic acids, including RNA helicases (Kelman et al. 1998; Jankowsky et al. 2000; Fairman-Williams and Jankowsky 2012). Many, if not all, of these enzymes start the reaction with one or more distributive steps before transitioning into a processive mode (Jankowsky et al. 2000). We speculate that this behavior is caused by conformational changes in the enzyme, reflecting conversion from a substrate binding mode to the processive mode where dissociation from the substrate is minimized.

An unusual feature of *S. cerevisiae* Pop2p, compared with other enzymes that work processively on RNA, is an impact of the initial substrate length on the extent of the processive phase. This observation implies a mechanism by which Pop2p senses the length of the substrate, although the molecular basis for this mechanism is not clear. Possible scenarios include rapid, one-dimensional diffusion of the enzyme prior to productive substrate engagement, transient oligomerization, or sensing of substrate length through conformational fluctuations of the unpaired RNA. Focused biophysical approaches are required to delineate the length-sensing mechanism(s). While cellular mRNAs are longer than the substrates tested in vitro, they are also bound to other proteins, form structures, or both. The accessible substrate length for cellular RNAs is thus likely to be considerably shorter than their actual length, and the observed length dependence of the processivity is likely to be reflected in cells, at least to some extent.

The third reaction phase of *S. cerevisiae* Pop2p, where processivity decreases, is not universally seen in other enzymes that processively work on RNA. This phase correlates, for some of the tested substrates, with the accumulation of the long terminal reaction products bearing a 3′-phosphate. It is possible that this correlation reflects a link between the alternative degradation pathways and the degree of processivity.

As noted, the most unusual feature of *S. cerevisiae* Pop2p is the ability to use two alternative degradation pathways—one cleaving 3′ and the other cleaving 5′ of the phosphate. Pop2p orthologs have not been reported to use alternative degradation pathways, although this might not have been examined for any of these enzymes. However, a human and a fly Pop2p ortholog do not produce the characteristic, long terminal reaction products, and generate only a single monophosphate (Bianchin et al. 2005; Niinuma et al. 2016). While it is not clear whether other Pop2p orthologs or other DEDD exonucleases use alternative degradation pathways, a unique mode of RNA degradation by *S. cerevisiae* Pop2p would be consistent with the noncanonical catalytic core of the enzyme (Thore et al. 2003; Winkler and Balacco 2013). Our data show that catalytic functionalities in the core are redundant and enzyme variants with one or two mutations show marked activity. Only substitutions of all five amino acids in the catalytic center reduce activity to near background. It is reasonable to assume that the redundancy of the catalytic functionalities contributes to the ability of *S. cerevisiae* Pop2p to use alternative degradation pathways.

In sum, our study reveals unusual features of the exonuclease Pop2p from *S. cerevisiae*. The observations show that exonucleases can harbor a spectrum of previously unappreciated functional diversity. Understanding the biochemical diversity of exonucleases appears important for developing a nuanced understanding of the cellular functions of these enzymes.

MATERIALS AND METHODS

Protein expression and purification

Full-length *S. cerevisiae pop2* was cloned into a pET-22b vector with an amino-terminal His_6-Sumo cleavable tag. All mutants used in this study were generated using the SLIM-PCR mutagenesis approach (Chiu et al. 2004). Sequences were verified by DNA sequencing. Proteins were expressed in *E. coli* (BL21) cells and induced by 0.5 mM Isopropyl β-D-1-thiogalactopyranoside (IPTG) at 19°C overnight. Cells were resuspended in lysis buffer containing 40 mM Tris (pH 8.0), 250 mM NaCl, 1 mM phenylmethylsulfonyl fluoride and 1 tablet of protease inhibitor cocktail (Roche). Cells were sonicated for 2 min and cellular debris were removed by ultracentrifugation and 15,000 rpm for 30 min. The cleared lysate was incubated with Ni^{2+} affinity beads at manufacturer's instruction for 2 h (Qiagen). Beads were washed with buffer containing 40 mM Tris (pH 8.0), 250 mM NaCl and 20 mM imidazole and proteins were eluted with 40 mM Tris (pH 8.0), 250 mM NaCl and 350 mM imidazole. Fractions containing Pop2p protein were then further purified by Mono-Q (GE Healthcare) anion exchange chromatography. Protein was applied to the column in 40 mM Tris (pH 8.0), 20 mM NaCl, followed by a wash with 40 mM Tris (pH 8.0), 100 mM NaCl, and eluted with 40 mM Tris (pH 8.0), 400 mM NaCl. Fractions containing Pop2p were pooled. The His_6-Sumo tag was then cleaved with Ulp1 sumo-protease at 4°C overnight (Mossessova and Lima 2000). The cleaved tags were removed from Pop2p by incubating the solution with Ni^{2+} affinity beads and collecting the flowthrough. Buffer was exchanged with a NAP-25 column (GE Healthcare) to 40 mM Tris (pH 8.0), 250 mM NaCl, 1 mM DTT, 20% (v/v) glycerol. Protein concentrations were determined with a spectrophotometer (280 nm) and further validated by Bradford assays. Aliquots (20–50 µL) of purified Pop2p were snap-frozen in liquid nitrogen and stored at −80°C.

RNA substrates

RNA substrates were purchased from Dharmacon and Sigma-Aldrich. RNA substrates were 5′ radiolabeled using γ^{32}P-ATP and T4 polynucleotide kinase (NEB). The internally radiolabeled substrate was generated by extending the A_{13} RNA with α^{32}P-ATP and *E. coli* poly(A) polymerase (NEB). Radiolabeled RNA substrates were purified with denaturing PAGE (acrylamide:bis 19:1, 7 M urea) and concentrations were quantified by scintillation counter (Srinivasan et al. 2020).

TABLE 1. Substrates used in exonuclease reactions

Name	Sequence (5′ → 3′)
A_{36}	5′AAAAAAAAAAAAAAAAAAAAAAAAAAAAAAAAAAAA
C_{36}	5′CCCCCCCCCCCCCCCCCCCCCCCCCCCCCCCCCCCC
U_{36}	5′UUUUUUUUUUUUUUUUUUUUUUUUUUUUUUUUUUUU
$A_{26}C_{10}$	5′AAAAAAAAAAAAAAAAAAAAAAAAAACCCCCCCCCC
$C_{26}A_{10}$	5′CCCCCCCCCCCCCCCCCCCCCCCCCCAAAAAAAAAA
AU-rich	5′UUAUUUAUUAUUUAUUUAUUUAUUAUUUAUUUAUUA
A_{24}	5′AAAAAAAAAAAAAAAAAAAAAAAA
C_{24}	5′CCCCCCCCCCCCCCCCCCCCCCCC
U_{24}	5′UUUUUUUUUUUUUUUUUUUUUUUU
A_{13}	5′AAAAAAAAAAAAA

Exonuclease reactions

Exonuclease activity reactions (20 µL) were conducted in a temperature-controlled aluminum block at 30°C in buffer containing 40 mM Tris (pH 8.0), 100 mM NaCl, 2 mM $MgCl_2$, 5% (v/v) glycerol, 2 mM DTT, 0.01% (v/v) NP-40, and 0.6 U/mL RNase Inhibitor (Roche). The reaction mix was incubated with indicated concentrations of Pop2p for 5 min. Reactions were started by addition of radiolabeled RNA substrate to final concentrations indicated. Aliquots were removed at specified time points and the reactions were quenched by addition of an equal volume of denaturing loading buffer (80% formamide, 0.025% [w/v] Xylene Cyanol and Bromophenol Blue). Samples were heated to 95°C, applied to 20% denaturing PAGE (acrylamide:bis 19:1, 7 M urea) and resolved to single nucleotide resolution. Gels were dried; the individual RNA species were visualized with Typhoon 9400 PhosphorImager (Amersham Biosciences) and quantified using ImageQuant 5.2 software (GE Healthcare).

Apparent reaction rate constant (k_{obs}) for degradation of the starting substrate at a given Pop2p concentration were calculated with the integrated rate law for an irreversible first order reaction.

$$A_{36}(t) = e^{-k_{obs}t}. \quad (1)$$

[$A_{36}(t)$: fraction RNA substrate at time t, k_{obs}: apparent reaction rate constant].

Pulse-chase reactions

Pulse-chase reactions were conducted under conditions identical to the pre-steady-state exonuclease reactions. Reactions were performed and allowed to proceed for a specified time (t_1), after which excess of unlabeled scavenger RNAs (same sequence as RNA substrate) was added to a final concentration of 5 µM. Control reactions were performed to confirm that the excess scavenger substrates completely prevented the rebinding of Pop2p to the radiolabeled substrates (Supplemental Fig. S2). Following scavenger addition, samples were allowed to react for another specified time (t_2), after which the reaction was terminated with denaturing loading buffer (as above). Samples were heated to 95°C, applied to denaturing PAGE (20% acrylamide:bis 19:1, 7 M urea) and resolved to single nucleotide resolution. Gels were dried, the individual RNA species were visualized with Typhoon 9400 PhosphorImager (Amersham Biosciences) and quantified using ImageQuant 5.2 software (GE Healthcare).

Processivity values for individual steps were calculated from the distribution of substrate species before and after pulse-chase, as previously described (Jia et al. 2011; Axhemi et al. 2020), according to:

$$\begin{cases} P_1 = 1 - \dfrac{A_0(t_1 + t_2)}{A_0(t_1)} \\ P_{i+1} = 1 - \dfrac{A_i(t_1 + t_2)}{A_i(t_1) + \sum_{j=0}^{i-1} A_j(t_1) \prod_{p=j+1}^{i} P_p} \; i = 1 \ldots n, \end{cases} \quad (2)$$

A_0 to A_i: relative concentrations of substrate species, P_1 to P_{i+1}: Processivity values of individual steps (P_1 corresponds to the processivity of the degradation of the first nucleotide, for example: $A_{36} \rightarrow A_{35}$). Processivity values were calculated via a Mathematica 6 script (Jia et al. 2011; Axhemi et al. 2020).

Thin layer chromatography (TLC)

Samples from the exonuclease reaction using internally radiolabeled RNA substrates at indicated time points were separated on a TLC cellulose plate (Sorbtech) in 0.1 M sodium phosphate buffer, pH 6.8/ammonium sulfate/n-propanol (100:60:2, v/w/v) or in 0.3 M LiCl and 0.5 M formic acid (Gu et al. 1997; Srinivasan et al. 2020). Following separation, TLC plates were dried and visualized with a Typhoon 9400 PhosphorImager. Species were quantified using the ImageQuant 5.2 software (GE Healthcare).

SUPPLEMENTAL MATERIAL

Supplemental material is available for this article.

ACKNOWLEDGMENTS

We thank Dr. Derek Taylor (CWRU) for sharing the pET-22b His_6-Sumo vector and Sumo protease. Purified *S. cerevisiae* Rrp44p was a generous gift by Dr. Christopher Lima (MSKCC, New York). We thank Dr. Xing-Huang Gao (CWRU) and Dr. Maria Hatzoglou (CWRU) for valuable discussions. This work

was supported by the National Institutes of Health (R35 GM118088 to E.J.).

Received October 5, 2020; accepted December 31, 2020.

REFERENCES

Andersen KR, Jonstrup AT, Van LB, Brodersen DE. 2009. The activity and selectivity of fission yeast Pop2p are affected by a high affinity for Zn^{2+} and Mn^{2+} in the active site. *RNA* **15:** 850–861. doi:10.1261/rna.1489409

Axhemi A, Wasmuth EV, Lima CD, Jankowsky E. 2020. Substrate selectivity by the exonuclease Rrp6p. *Proc Natl Acad Sci* **117:** 982–992. doi:10.1073/pnas.1913236117

Balagopal V, Bolisetty M, Al Husaini N, Coller J, Graveley BR. 2017. Ccr4 and Pop2 control poly(A) tail length in *Saccharomyces cerevisiae*. bioRxiv. doi:10.1101/140202

Basquin J, Roudko VV, Rode M, Basquin C, Seraphin B, Conti E. 2012. Architecture of the nuclease module of the yeast Ccr4-not complex: the Not1-Caf1-Ccr4 interaction. *Mol Cell* **48:** 207–218. doi:10.1016/j.molcel.2012.08.014

Bianchin C, Mauxion F, Sentis S, Seraphin B, Corbo L. 2005. Conservation of the deadenylase activity of proteins of the Caf1 family in human. *RNA* **11:** 487–494. doi:10.1261/rna.7135305

Chiu J, March PE, Lee R, Tillett D. 2004. Site-directed, ligase-independent mutagenesis (SLIM): a single-tube methodology approaching 100% efficiency in 4 h. *Nucleic Acids Res* **32:** e174. doi:10.1093/nar/gnh172

Collart MA, Panasenko OO. 2017. The Ccr4-Not complex: architecture and structural insights. *Subcell Biochem* **83:** 349–379. doi:10.1007/978-3-319-46503-6_13

Das U, Shuman S. 2013. Mechanism of RNA 2′,3′-cyclic phosphate end healing by T4 polynucleotide kinase-phosphatase. *Nucleic Acids Res* **41:** 355–365. doi:10.1093/nar/gks977

Daugeron M, Mauxion F, Séraphin B. 2001. The yeast POP2 gene encodes a nuclease involved in mRNA deadenylation. *Nucleic Acids Res* **29:** 2448–2455. doi:10.1093/nar/29.12.2448

Fairman-Williams M, Jankowsky E. 2012. Unwinding initiation by the viral RNA helicase NPH-II. *J Mol Biol* **415:** 819–832. doi:10.1016/j.jmb.2011.11.045

Gu J, Shumyatsky G, Makan N, Reddy R. 1997. Formation of 2′,3′-cyclic phosphates at the 3′ end of human U6 small nuclear RNA in vitro. Identification of 2′,3′-cyclic phosphates at the 3′ ends of human signal recognition particle and mitochondrial RNA processing RNAs. *J Biol Chem* **272:** 21989–21993. doi:10.1074/jbc.272.35.21989

Horiuchi M, Takeuchi K, Noda N, Muroya N, Suzuki T, Nakamura T, Kawamura-Tsuzuku J, Takahasi K, Yamamoto T, Inagaki F. 2009. Structural basis for the antiproliferative activity of the Tob-hCaf1 complex. *J Biol Chem* **284:** 13244–13255. doi:10.1074/jbc.M809250200

Ibrahim H, Wilusz J, Wilusz C. 2009. RNA recognition by 3′-to-5′ exonucleases: the substrate perspective. *Biochim Biophys Acta* **1779:** 256–265. doi:10.1016/j.bbagrm.2007.11.004

Jankowsky E, Gross CH, Shuman S, Pyle AM. 2000. The DExH protein NPH-II is a processive and directional motor for unwinding RNA. *Nature* **403:** 447–451. doi:10.1038/35000239

Jia H, Wang X, Liu F, Guenther UP, Srinivasan S, Anderson JT, Jankowsky E. 2011. The RNA helicase Mtr4p modulates polyadenylation in the TRAMP complex. *Cell* **145:** 890–901. doi:10.1016/j.cell.2011.05.010

Jonstrup AT, Andersen KR, Van LB, Brodersen DE. 2007. The 1.4-A crystal structure of the *S. pombe* Pop2p deadenylase subunit unveils the configuration of an active enzyme. *Nucleic Acids Res* **35:** 3153–3164. doi:10.1093/nar/gkm178

Kelman Z, Hurwitz J, Donnell M. 1998. Processivity of DNA polymerases: two mechanisms, one goal. *Structure* **6:** 121–125. doi:10.1016/S0969-2126(98)00014-8

Mossessova E, Lima CD. 2000. Ulp1-SUMO crystal structure and genetic analysis reveal conserved interactions and a regulatory element essential for cell growth in yeast. *Mol Cell* **5:** 865–876. doi:10.1016/S1097-2765(00)80326-3

Niinuma S, Fukaya T, Tomari Y. 2016. CCR4 and CAF1 deadenylases have an intrinsic activity to remove the post-poly(A) sequence. *RNA* **22:** 1550–1559. doi:10.1261/rna.057679.116

Parker R. 2012. RNA degradation in *Saccharomyces cerevisiae*. *Genetics* **191:** 671–702. doi:10.1534/genetics.111.137265

Raisch T, Chang CT, Levdansky Y, Muthukumar S, Raunser S, Valkov E. 2019. Reconstitution of recombinant human CCR4-NOT reveals molecular insights into regulated deadenylation. *Nat Commun* **10:** 3173. doi:10.1038/s41467-019-11094-z

Rina M, Pozidis C, Mavromatis K, Tzanodaskalaki M, Kokkinidis M, Bouriotis V. 2000. Alkaline phosphatase from the Antarctic strain TAB5. *Eur J Biochem* **267:** 1230–1238. doi:10.1046/j.1432-1327.2000.01127.x

Schwede A, Ellis L, Luther J, Carrington M, Stoecklin G, Clayton C. 2008. A role for Caf1 in mRNA deadenylation and decay in trypanosomes and human cells. *Nucleic Acids Res* **36:** 3374–3388. doi:10.1093/nar/gkn108

Sengar A, Heddi B, Phan AT. 2014. Formation of G-quadruplexes in poly-G sequences: structure of a propeller-type parallel-stranded G-quadruplex formed by a G_{15} stretch. *Biochemistry* **53:** 7718–7723. doi:10.1021/bi500990v

Srinivasan S, Liu Z, Chuenchor W, Xiao TS, Jankowsky E. 2020. Function of auxiliary domains of the DEAH/RHA helicase DHX36 in RNA remodeling. *J Mol Biol* **432:** 2217–2231. doi:10.1016/j.jmb.2020.02.005

Tang TTL, Passmore LA. 2019. Recognition of poly(A) RNA through its intrinsic helical structure. *Cold Spring Harb Symp Quant Biol* **84:** 21–30. doi:10.1101/sqb.2019.84.039818

Tang TTL, Stowell JAW, Hill CH, Passmore LA. 2019. The intrinsic structure of poly(A) RNA determines the specificity of Pan2 and Caf1 deadenylases. *Nat Struct Mol Biol* **26:** 433–442. doi:10.1038/s41594-019-0227-9

Temme C, Zaessinger S, Meyer S, Simonelig M, Wahle E. 2004. A complex containing the CCR4 and CAF1 proteins is involved in mRNA deadenylation in *Drosophila*. *EMBO J* **23:** 2862–2871. doi:10.1038/sj.emboj.7600273

Temme C, Zhang L, Kremmer E, Ihling C, Chartier A, Sinz A, Simonelig M, Wahle E. 2010. Subunits of the *Drosophila* CCR4-NOT complex and their roles in mRNA deadenylation. *RNA* **16:** 1356–1370. doi:10.1261/rna.2145110

Thore S, Mauxion F, Seraphin B, Suck D. 2003. X-ray structure and activity of the yeast Pop2 protein: a nuclease subunit of the mRNA deadenylase complex. *EMBO Rep* **4:** 1150–1155. doi:10.1038/sj.embor.7400020

Tucker M, Valencia-Sanchez M, Staples R, Chen J, Denis C, Parker R. 2001. The transcription factor associated Ccr4 and Caf1 proteins are components of the major cytoplasmic mRNA deadenylase in *Saccharomyces cerevisiae*. *Cell* **104:** 377–386. doi:10.1016/S0092-8674(01)00225-2

Tucker M, Staples R, Valencia-Sanchez M, Muhlrad D, Parker R. 2002. Ccr4p is the catalytic subunit of a Ccr4p/Pop2p/Notp mRNA deadenylase complex in *Saccharomyces cerevisiae*. *EMBO J* **21:** 1427–1436. doi:10.1093/emboj/21.6.1427

Viswanathan P, Ohn T, Chiang YC, Chen J, Denis CL. 2004. Mouse CAF1 can function as a processive deadenylase/3′-5′-exonuclease

in vitro but in yeast the deadenylase function of CAF1 is not required for mRNA poly(A) removal. *J Biol Chem* **279:** 23988–23995. doi:10.1074/jbc.M402803200

Webster MW, Chen YH, Stowell JAW, Alhusaini N, Sweet T, Graveley BR, Coller J, Passmore LA. 2018. mRNA deadenylation is coupled to translation rates by the differential activities of Ccr4-Not nucleases. *Mol Cell* **70:** 1089–1100.e1088. doi:10.1016/j.molcel.2018.05.033

Winkler GS, Balacco DL. 2013. Heterogeneity and complexity within the nuclease module of the Ccr4-Not complex. *Front Genet* **4:** 296. doi:10.3389/fgene.2013.00296

Yi H, Park J, Ha M, Lim J, Chang H, Kim VN. 2018. PABP cooperates with the CCR4-NOT complex to promote mRNA deadenylation and block precocious decay. *Mol Cell* **70:** 1081–1088.e1085. doi:10.1016/j.molcel.2018.05.009

Zinder JC, Wasmuth EV, Lima CD. 2016. Nuclear RNA exosome at 3.1 A reveals substrate specificities, RNA paths, and allosteric inhibition of Rrp44/Dis3. *Mol Cell* **64:** 734–745. doi:10.1016/j.molcel.2016.09.038

Zuo Y, Deutscher M. 2001. Exoribonuclease superfamilies: structural analysis and phylogenetic distribution. *Nucleic Acids Res* **29:** 1017–1026. doi:10.1093/nar/29.5.1017